Dynamics of extended space charge in concentration polarization

Isaak Rubinstein* and Boris Zaltzman†

Blaustein Institutes for Desert Research, Ben-Gurion University of the Negev, Sede Boqer Campus, Midreshet Ben-Gurion 84990, Israel

(Received 3 April 2010; published 17 June 2010)

This paper is concerned with ionic currents from an electrolyte solution into a charge selective solid, such as an electrode, an ion exchange membrane or an array of nanochannels in a microfluidic system. All systems of this kind have characteristic voltage-current curves with segments in which current nearly saturates at some plateau values due to concentration polarization—formation of solute concentration gradients under the passage of a dc current. A number of seemingly different phenomena occurring in that range, such as anomalous rectification in cathodic copper deposition from a copper sulfate solution, superfast vortexes near an ion-exchange granule, overlimiting conductance in electrodialysis and the recently observed nonequilibrium electro-osmotic instability, result from formation of an additional extended space charge layer next to that of a classical electrical double layer at the solid/liquid interface or, rather, from the peculiar features of the extended space charge distinguishing it from that of a common diffuse electrical double layer. In this paper we discuss the nature and origin of the extended space charge and analyze its peculiar steady state and time-dependent properties important for understanding nonequilibrium electrokinetic phenomena in ionic systems.

DOI: 10.1103/PhysRevE.81.061502 PACS number(s): 82.45.Gj, 82.45.Fk

I. INTRODUCTION

In our recent studies [1,2] we re-examined the electrodiffusion time scales near the equilibrium (Ref. [1]) and assessed the possibility of probing the diffuse electrical double layer (EDL) at a permeable charge-selective interface, such as a nonblocking electrode with a local equilibrium, ion-exchange membrane, or an array of nanochannels, under a finite steady-state current or voltage bias by small harmonic high frequency current or voltage disturbances, electrical impedance spectroscopy (EIS) (Ref. [2]).

Our main conclusion in Ref. [1] was that near the equilibrium the EDL at such interfaces, as opposed to that at a blocking interface, is essentially unamenable to the aforementioned probing, with the entire system's high-frequency response dominated by the quasielectroneutral bulk (QEB). In the follow-up paper [2] we addressed the same question away from equilibrium—under a finite steady-state current or voltage bias. We particularly focused on the issue of probing the extended space charge (ESC) forming in such EDLs in binary electrolytes in the course of concentration polarization (CP) near the limiting current (LC) [3–19]. This ESC is the source of nonequilibrium electrokinetic effects of the second kind [11–20], including formation of the Dukhin's vortices [13] and nonequilibrium electro-osmotic instability in ionic conductance [11,12,18]. This makes direct experimental probing of the ESC a relevant task especially in view of the fact that, the aforementioned effects likely control several processes of considerable applied importance, such as overlimiting conductance in electrodialysis and shock formation in protein preconcentration in micronanochannel systems [21–23]. In this regime, corresponding to extreme electrolyte depletion, the classical Poisson-Nernst-Planck description of electrodiffusion is suitable without a need to account for steric effects relevant for high ionic concentrations [24,25]. The analysis in [2] was performed upon the same nonblocking model problems as previously [1]. The main conclusion was that also for a finite underlimiting bias, like near the equilibrium, EDL at a nonblocking interface is not amenable to this kind of probe; the high-frequency response of the system is still dominated by QEB. On the other hand, ESC in such EDLs may be probed in this way both by the linear and nonlinear response, correspondingly by the EIS method and via the anomalous rectification (AR) effect [26,27]. The latter appears preferable over the former as a potential experimental tool for the study of ESC. Historically, until the discovery of the nonequilibrium electrokinetic effects of the second kind, AR remained the only known macroscopic "footprint" of ESC in CP. It was argued in [2] that both nonequilibrium electro-osmotic instability and AR are expressions of the same feature of ESC of nonequilibrium EDL (NE-EDL) distinguishing it from the common diffuse space charge of quasiequilibrium EDL (QE-EDL).

This paper complements the above mentioned previous studies [1,2] by addressing the peculiarity of NE-EDL and ESC fronts. The main questions addressed here are as follows: what is ESC? Is it just the external part of a stretched distorted EDL or something else, an entirely new structure only spatially adjacent to EDL? If the former, the membrane being an essentially bottomless source of counterions, what could be the force pooling them out of it, while the electric force pushes them back?

Below we conclude that ESC is not a part of EDL, rather it is an extended vicinity of the counterions concentration minimum with coions expelled from it by the electric field. This conclusion emerges from a rigorous steady-state analysis of the EDL structure in a one-dimensional (1D) model of the diffusion layer at an ideally permselective membrane (Sec. II) and study of the charge dynamics in this problem combined with the observations on this system's time response to an instantaneous voltage increment (Sec. III). In addition, it is observed that ESC would even form without an equilibrium EDL, with coions just sterically prohibited from

*robinst@bgu.ac.il
†boris@bgu.ac.il

entering the membrane, as in the "toy" model discussed in Appendix A.

In Sec. IV we generalize the EDL analysis for a more realistic three-layer problem, modeling a nonideally permselective membrane flanked by two electrolyte diffusion layers. For the purpose of analyzing the effect of membrane selectivity on the dynamics of QE-EDL and ESC at the depleted membrane/solution interface, in Sec. V the three-layer model of Sec. IV is reduced to a much simpler one-layer setup.

For reference, in Appendix B we recapitulate from Ref. [19] various types of the EDL's structure corresponding to various ranges of the applied voltage in relation to the dimensionless Debye length $\varepsilon \ll 1$, resulting from a suitable analysis of the Painleve equation for the electric field in the EDL.

II. FINE EDL STRUCTURE IN 1D STEADY-STATE MODEL PROBLEM FOR IDEALLY PERMSELECTIVE MEMBRANE

Below we analyze the following 1D steady-state model problem. Let us consider a diffusion layer $0<x<1$ of a univalent electrolyte flanked by an ideal permselective membrane (ideal nonblocking electrodes) $x=0$ and by a stirred bulk solution maintained a fixed electrolyte concentration and zero electric potential at $x=1$. The corresponding boundary value problem reads

$$\overset{\text{def}}{j^+} = (c_x^+ + c^+\varphi_x) = \text{const}, \tag{1}$$

$$\overset{\text{def}}{j^-} = (c_x^- - c^-\varphi_x) = 0, \tag{2}$$

$$\varepsilon^2\varphi_{xx} = c^- - c^+, \tag{3}$$

$$\varphi(0) = -V, \quad \varphi(1) = 0, \tag{4}$$

$$c^+(0) = p_1, \tag{5}$$

$$c^-(1) = 1, \quad c^+(1) = 1. \tag{6}$$

Here c^+ and c^- are the dimensionless concentrations of cations (counterions) and anions (coions), respectively (normalized by the "outer" stirred bulk concentration c_0); φ is the dimensionless electric potential (normalized by the thermal potential RT/F); x is the dimensionless spatial coordinate (normalized by the diffusion layer thickness L) and j^+, j^- are the dimensionless ionic fluxes (with a minus sign); V is a dimensionless voltage bias applied between the stirred bulk and the membrane. Equations (1) and (2) are the steady-state Nernst-Planck-Einstein equations for counterions and coions, respectively, Eq. (3) is the Poisson equation with the space charge in the right-hand side due to the local ionic concentration imbalance and ε is the dimensionless Debye length defined as

$$\varepsilon = \frac{(dRT)^{1/2}}{2F(\pi c_0)^{1/2}L}, \tag{7}$$

where F is the Faraday constant, R is the universal gas constant, T is the absolute temperature, and d is the dielectric constant of the solution. ε^2 lies in the range $2\times10^{-13}<\varepsilon^2<2\times10^{-5}$, for a realistic macroscopic system with $10^{-4}<L(\text{cm})<10^{-1}$, $10^{-4}<c_0(\text{mol})<1$. Equation (2) asserts impermeability of the membrane for coions, whereas Eq. (5) fixes the counterion concentration at the membrane/solution interface. $p_1=\frac{N}{e}\gg 1$, where N is the dimensionless fixed charge density in the membranes and V is a constant dimensionless voltage bias applied between the stirred bulk and the membrane. Condition (6) specifies the dimensionless concentration at the outer edge of the diffusion layer at unity. Assuming ε constant, with the underlying implicit assumption of a constant dielectric permeability, is of course a crude approximation in the current analysis [28] to be relaxed in future studies.

By defining

$$\overset{\text{def}}{E} = -\varepsilon\frac{d\varphi}{dx} \tag{8}$$

and adding Eq. (1) into Eq. (3), we rewrite Eqs. (1)–(3) as follows:

$$E(c^+ + c^-) = \varepsilon\frac{d}{dx}(c^+ - c^-) - \varepsilon j^+, \tag{9}$$

$$c^+ - c^- = \varepsilon\frac{dE}{dx}, \tag{10}$$

$$\varepsilon\frac{dc^+}{dx} = Ec^+ + \varepsilon j^+. \tag{11}$$

By adding Eq. (9) into Eq. (10) multiplied by E, substituting c^+-c^- from Eq. (10) and c^+E from Eq. (11) and integrating the resulting equation, we obtain

$$c^+ = \frac{\varepsilon}{2}\frac{dE}{dx} + \frac{1}{4}E^2 + \frac{j^+}{2}(x - x_0). \tag{12}$$

Here x_0 is an integration constant, which is the root of the linear extrapolation of the outer QEB ionic concentration profile near the interface. By substituting Eq. (12) into Eq. (11) we obtain the following inhomogeneous Painleve equation of the second kind for E:

$$\varepsilon^2\frac{d^2E}{dx^2} = \frac{1}{2}E^3 + j^+(x - x_0)E + \varepsilon j^+. \tag{13}$$

To analyze Eq. (12), we define the following boundary layer variables F and z:

$$\overset{\text{def}}{F} = (j^+)^{-1/3}\varepsilon^{-1/3}, \quad \overset{\text{def}}{z} = (j^+)^{1/3}\varepsilon^{-2/3}x. \tag{14}$$

In terms of these variables, the boundary value problem [Eqs. (1)–(6)] assumes the form

$$\frac{d^2F}{dz^2} = \frac{1}{2}F^3 + (z - z_0)F + 1, \quad 0 < z, \tag{15}$$

$$\left(\frac{dF}{dz} + \frac{1}{2}F^2\right)\Big|_{z=0} = 2(j^+)^{-2/3}\varepsilon^{-2/3}p_1 + z_0, \tag{16}$$

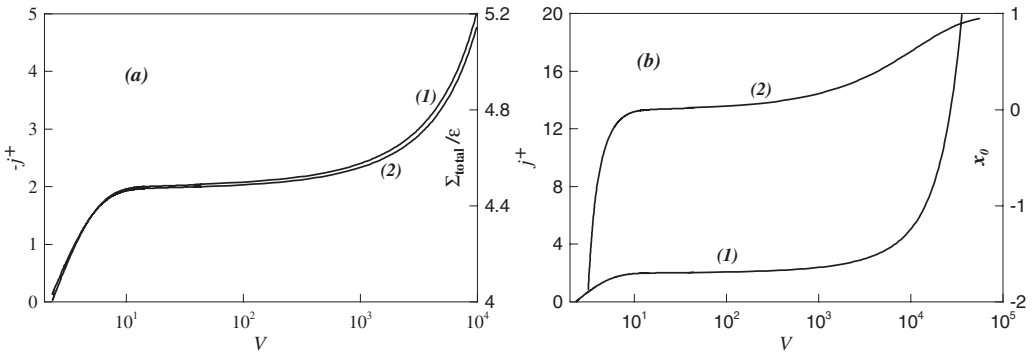

FIG. 1. (a) Current (curve 1), total charge (curve 2)-voltage dependence and (b) current (curve 1), normalized vanishing concentration location x_0 (curve 2)—voltage dependence; one-layer model, $p_1=10$, $\varepsilon=0.0001$. The voltage range unrealistically extended for completeness of mathematical picture of ESC.

$$F(z) = -\frac{1}{z - z_0} \quad \text{for} \quad z \gg z_0(\text{QEB}), \tag{17}$$

$$\lim_{z\to\infty}\left(\int_0^z F(z)dz + \ln(z - z_0)\right) = -\frac{2}{3}\ln\varepsilon - \frac{2}{3}\ln j^+ - V + \ln 2. \tag{18}$$

Here parameter z_0 is defined as

$$z_0 = (j^+)^{1/3}\varepsilon^{-2/3}x_0, \tag{19}$$

and the electric current j^+ is determined by solution of a suitable problem. Solution of the problem [Eqs. (14)–(18)] and its related uniformly valid description of the EDL under current in various voltage regimes was given in Ref. [19]. For future reference, in Appendix B, we reproduce from Ref. [19] various types of solutions to the Painleve Eq. (15) and its approximations, corresponding to various ranges of parameter $z_0(\varepsilon)$ and, thus, through Eq. (18), to various ranges of voltage V in relation to $\varepsilon \ll 1$.

III. CHARGE DYNAMICS IN 1D STEADY-STATE MODEL PROBLEM FOR IDEALLY PERMSELECTIVE MEMBRANE

We begin with analyzing the dependence on V for various regimes of EDL of the total charge in the diffusion layer defined as

$$\Sigma_{\text{total}} \overset{\text{def}}{=} \int_0^1 (c^+ - c^-)dx = \varepsilon^2\varphi_x(0) + O(\varepsilon^2). \tag{20}$$

Solution of the problem [Eqs. (15)–(18)] for the quasiequilibrium range (underlimiting current regime), $V \ll \frac{4}{3}|\ln\varepsilon|$, $-z_0 \gg 1$, yields to leading order [19],

$$\Sigma_{\text{total}} = \frac{\varepsilon}{\sqrt{2p_1}}(x_0 j^+ + 2p_1) = \varepsilon\sqrt{\frac{2}{p_1}}(p_1 - \bar{c}(0)), \tag{21}$$

where $\bar{c}(0) = 1 - j^+/2$ is the value of the outer QEB concentration at the membrane/solution interface. In Fig. 1(a) we plot the current (j^+)–voltage (V) dependence (curve 1) along with the total charge (Σ_{total})–voltage (V) dependence (curve 2). We note the saturation in both plots for the intermediate high voltage–strong depletion ($\bar{c}(0) \to 0$) range. In Fig. 1(b) we reproduce once more the current (j^+)-voltage (V) dependence (curve 1) along with that of the parameter z_0 (curve 2). We note that current saturation in curve 1 is accompanied by z_0 changing sign, thus manifesting the appearance of ESC.

For the nonequilibrium range $\frac{4}{3}|\ln\varepsilon| \le O(V) < \frac{1}{\varepsilon}$, $1 \le O(z_0) < \frac{1}{\varepsilon^{2/3}}$ analysis of Eqs. (15)–(18) yields to leading order,

$$\Sigma_{\text{total}} = \varepsilon\sqrt{2p_1}. \tag{22}$$

Finally, for the macroscopic ESC regime, $V = O(\frac{1}{\varepsilon})$, $z_0 = O(\frac{1}{\varepsilon})$, Eqs. (15)–(18) yield to the leading order, see Ref. [19],

$$\Sigma_{\text{total}} = \varepsilon\sqrt{2p_1 + 2x_0 j^+} = \frac{\varepsilon}{\sqrt{2p_1}}[(x_0 j^+ + 2p_1) + O(x_0^2)], \tag{23}$$

which corresponds to the inflexion and 'second rise' of the current and the total charge in Figs. 1(a) and 1(b) in the extremely high-voltage range. Of course this range ($10^2 V - 10^3 V$ in dimensional variables compared to no more than a few volts or, rather, fractions of a volt in realistic situations) is of mathematical interest only and its related "second rise" has nothing to do with the true mechanism of overlimiting conductance. We note that all three Eqs. (21)–(23) are identical to the leading-order term for the limiting current regime $|x_0| \ll 1$.

In Figs. 2(a) and 2(b) we compare the numerically computed total charge Σ_1 with that given by Eq. (23). We note that both stand in a very good agreement not only for the extreme macroscopic ESC regime, $z_0 = O(\varepsilon^{-2/3})$, but also for finite positive values of z_0 and, correspondingly, moderate voltages, $V \sim |\frac{4}{3}\ln\varepsilon|$.

Summarizing, with the current at the limiting value while ESC is forming, the total charge remains practically unchanged up to very high voltages of the order of $O(\frac{1}{\varepsilon})$. After that the total charge starts to increase again in accordance with Eq. (23) as illustrated in Fig. 1(a).

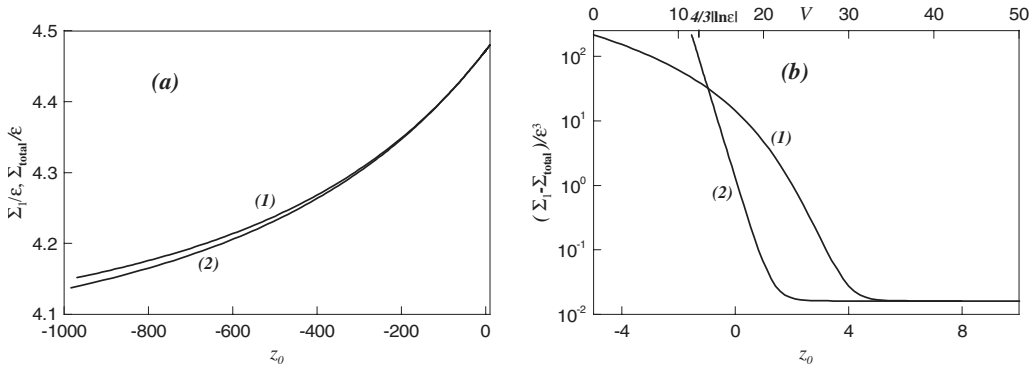

FIG. 2. Comparison of the numerically calculated total charge Σ_1 with its asymptotic approximation Σ_{total} (a) Σ_{total} (curve 1), Σ_1 (curve 2) versus parameter z_0; (b) the ratio $\Sigma_1-\Sigma_{total}/\varepsilon^3$ versus parameter z_0, curve 1; and versus voltage V, curve 2; $p_1=10$, $\varepsilon=0.0001$.

In the rest of this section we discuss the fine structure of the EDL under current and the charge dynamics in conditions of CP. We begin with describing the charge distribution in the EDL for various regimes. In Fig. 3(a) we present the charge distribution plots,

$$\Sigma(x) \overset{\text{def}}{=} \int_x^1 (c^+ - c^-)dx = \varepsilon^2\varphi_x(x) + O(\varepsilon^2), \tag{24}$$

for a sequence of values of the parameter z_0 and the corresponding voltage V. Let us note that for $z_0>0$ ESC is partly formed at the expense of QE-EDL. The considerable part of ESC is located in the transition zone to QEB. This manifests itself via the appearance in this zone of a charge-density front with another charge-density maximum, in addition to that at the solution/membrane interface ($x=0$). This is illustrated in Fig. 3(b) depicting the charge-density profiles.

In Fig. 4(a) we present two more plots illustrating the total charge saturation at the limiting current and its relative shift from the QE-EDL to the ESC zone. For this purpose, let us define the QE-EDL outer edge as the location of the cation concentration minimum, x_{min}:

$$x_{min}: \frac{dc^+}{dx}(x_{min}) = 0, \tag{25}$$

with the QE-EDL charge $\Sigma_{QE\text{-}EDL}$ and ESC Σ_{ESC} defined accordingly as

$$\Sigma_{QE\text{-}EDL} \overset{\text{def}}{=} \int_0^{x_{min}} (c^+ - c^-)dx = \varepsilon^2[\varphi_x(0) - \varphi_x(x_{min})], \tag{26}$$

$$\Sigma_{ESC} \overset{\text{def}}{=} \int_{x_{min}}^1 (c^+ - c^-)dx = \varepsilon^2\varphi_x(x_{min}) + O(\varepsilon^2). \tag{27}$$

The first curve in Fig. 4(a), illustrating the total charge saturation, depicts the convergence with the increasing voltage of the total charge Σ_{total} to its limiting value $\varepsilon\sqrt{2p_1}$ with an accuracy $\varepsilon^{5/3}$. The second curve illustrates the parallel monotonic increase in ESC Σ_{ESC}.

To identify the precise mechanism behind this redistribution of the total charge, we trace the counterion and coion redistribution with the voltage increase. In Fig. 4(b) we present the ionic concentration profiles for an increasing sequence of parameter z_0 with voltage V. We note the decrease in both concentrations with the increasing voltage and a parallel expansion of the cation concentration minimum zone into a finite-size interval (finite-size ESC region), practically void of coions. This suggests the following picture of the systems response to increasing voltage. As a result of an increase in the electric field acting in the direction of the membrane the counterions are being pushed and leave the EDL in the opposite direction toward the bulk. Near the equi-

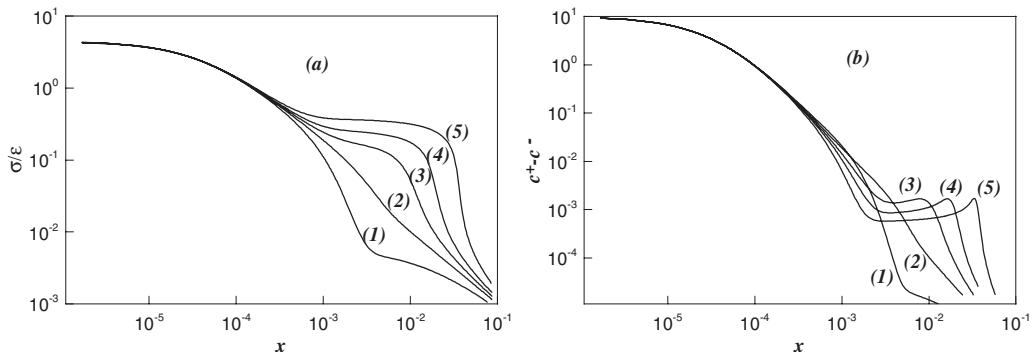

FIG. 3. (a) Charge Σ distribution plots for a sequence of voltages V, parameter z_0 values: 1—$z_0=-10$, $V=9.44$ (QE-EDL), 2—$z_0=0$, $V=13.94$ (transitional regime to NE-EDL), 3—$z_0=5$, $V=23.38$ (appearance of ESC), 4—$z_0=10$, $V=42.31$ (NE-EDL), 5—$z_0=20$, $V=96.5$ (NE-EDL); $p_1=10$, $\varepsilon=0.0001$; (b) charge-density c^+-c^- plots for a sequence of voltages V, parameter z_0 values: 1—$z_0=-10$, $V=9.44$ (QE-EDL), 2—$z_0=0$, $V=13.94$ (transitional regime to NE-EDL), 3—$z_0=5$, $V=23.38$ (appearance of the ESC), 4—$z_0=10$, $V=42.31$ (NE-EDL), 5—$z_0=20$, $V=96.5$ (NE-EDL); $p_1=10$, $\varepsilon=0.0001$.

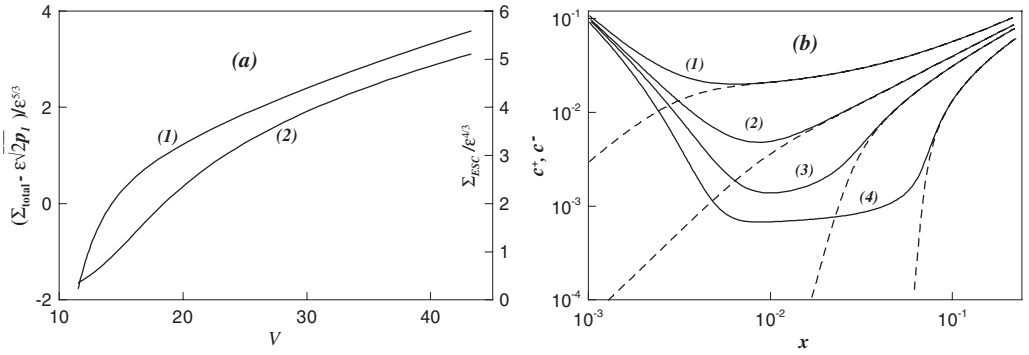

FIG. 4. (a) The dependence of the total charge deviation from its limiting value, $\Sigma_{\text{total}}-\varepsilon\sqrt{2p_1}$, as a function on the applied voltage V, curve 1; and the dependence of the ESC Σ_{ESC} on the applied voltage V, curve 2; $p_1=10$, $\varepsilon=0.0001$. (b) Cation c^+ (continuous line) and anion c^- (dashed line) profiles for a sequence of voltages V (and the corresponding values of parameter z_0): (1) $z_0=-10$, $V=9.44$ (QE-EDL), (2) $z_0=0$, $V=13.94$ (transitional regime to NE-EDL), (3) $z_0=5$, $V=23.38$ (appearance of ESC), and (4) $z_0=15$, $V=68$ (NE-EDL); $p_1=10$, $\varepsilon=0.0001$.

librium, the coions concentration decreases faster than that of counterions, yielding an increase in the total charge of the QE-EDL. Upon the expulsion of coions near the limiting current, the QE-EDL starts shrinking both in thickness and in terms of its charge. Simultaneously, with the coions expelled from it by the electric field, the locus of the counterion concentration minimum expands to a zone of a finite size, giving rise to the emergence of ESC. The latter is in a nonequilibrium charged entity which develops next to QE-EDL partly at its expense. At its emergence, the total ESC is of the order of $\varepsilon^{4/3}$ and is mainly concentrated in a $\varepsilon^{2/3}$ wide charge front zone between ESC and the QEB solution.

This qualitative picture stands in line with the following asymptotic steady-state arguments valid for the moderate voltage or underlimiting current regime. For these conditions, the following Boltzmann relations for the ionic concentrations are valid in QE-EDL, $0<x\leq O(\varepsilon)$:

$$c^- = e^{\varphi}, \quad c^+ = \bar{c}(0)^2 e^{-\varphi} = \left(1-\frac{j^+}{2}\right)^2 e^{-\varphi}. \tag{28}$$

Substituting Eq. (27) into the Poisson Eq. (3) and integrating the obtained equation we find

$$\varphi = \ln \bar{c}(0) + 2\ln\frac{\sqrt{\bar{c}(0)}+\sqrt{p_1}-(\sqrt{p_1}-\sqrt{\bar{c}(0)})e^{-x/\varepsilon\sqrt{2\bar{c}(0)}}}{\sqrt{\bar{c}(0)}+\sqrt{p_1}+(\sqrt{p_1}-\sqrt{\bar{c}(0)})e^{-x/\varepsilon\sqrt{2\bar{c}(0)}}}. \tag{29}$$

Substituting Eq. (27) into the Poisson Eq. (3) and integrating the obtained equation we find

$$\varphi = \ln \bar{c}(0) + 2\ln\frac{\sqrt{\bar{c}(0)}+\sqrt{p_1}-(\sqrt{p_1}-\sqrt{\bar{c}(0)})e^{-x/\varepsilon\sqrt{2\bar{c}(0)}}}{\sqrt{\bar{c}(0)}+\sqrt{p_1}+(\sqrt{p_1}-\sqrt{\bar{c}(0)})e^{-x/\varepsilon\sqrt{2\bar{c}(0)}}}. \tag{30}$$

Substitution of Eq. (29) into Eq. (28) yields for $0<x\leq O(\varepsilon)$:

$$c^- = \bar{c}(0)\left(\frac{\sqrt{\bar{c}(0)}+\sqrt{p_1}-(\sqrt{p_1}-\sqrt{\bar{c}(0)})e^{-x/\varepsilon\sqrt{2\bar{c}(0)}}}{\sqrt{\bar{c}(0)}+\sqrt{p_1}+(\sqrt{p_1}-\sqrt{\bar{c}(0)})e^{-x/\varepsilon\sqrt{2\bar{c}(0)}}}\right)^2, \tag{31}$$

$$c^+ = \bar{c}(0)\left(\frac{\sqrt{\bar{c}(0)}+\sqrt{p_1}+(\sqrt{p_1}-\sqrt{\bar{c}(0)})e^{-x/\varepsilon\sqrt{2\bar{c}(0)}}}{\sqrt{\bar{c}(0)}+\sqrt{p_1}-(\sqrt{p_1}-\sqrt{\bar{c}(0)})e^{-x/\varepsilon\sqrt{2\bar{c}(0)}}}\right)^2. \tag{32}$$

Combining the "inner" cationic concentration [Eq. (32)] with the "outer" ionic concentration in the electroneutral bulk yields the following composite expression for the cation concentration valid in the entire diffusion layer, $0\leq x\leq 1$,

$$c^+ = \bar{c}(0)\left(\frac{\sqrt{\bar{c}(0)}+\sqrt{p_1}+(\sqrt{p_1}-\sqrt{\bar{c}(0)})e^{-x/\varepsilon\sqrt{2\bar{c}(0)}}}{\sqrt{\bar{c}(0)}+\sqrt{p_1}-(\sqrt{p_1}-\sqrt{\bar{c}(0)})e^{-x/\varepsilon\sqrt{2\bar{c}(0)}}}\right)^2 + \frac{j^+}{2}x. \tag{33}$$

Finding the location of the minimum cation concentration from Eq. (33) yields for the outer edge of the QE-EDL the expression

$$x_{\min} = \frac{\varepsilon}{\sqrt{2\bar{c}(0)}}\left(\frac{3}{2}\ln\frac{2\bar{c}(0)}{\varepsilon^{2/3}} + \ln\frac{4}{j^+} + \ln\frac{\sqrt{p1}-\sqrt{\bar{c}(0)}}{\sqrt{p1}+\sqrt{\bar{c}(0)}}\right). \tag{34}$$

With the ionic masses in the QE-EDL defined as

$$\sigma^+ \overset{\text{def}}{=} \int_0^{x_{\min}} c^+ dx, \quad \sigma^- \overset{\text{def}}{=} \int_0^{x_{\min}} c^- dx, \tag{35}$$

Eqs. (31)–(34) yield for $j^+<2$, $V=O(1)$ to the leading order:

$$\frac{\sigma^-}{\varepsilon} = \frac{\sqrt{2\bar{c}(0)}}{2}\left(\frac{3}{2}\ln\frac{2\bar{c}(0)}{\varepsilon^{2/3}} + \ln\frac{4}{j^+} + \ln\frac{\sqrt{p1}-\sqrt{\bar{c}(0)}}{\sqrt{p1}+\sqrt{\bar{c}(0)}}\right), \tag{36}$$

$$\frac{\sigma^+}{\varepsilon} = \frac{\sigma^-}{\varepsilon} + \sqrt{2p_1} - \sqrt{2\bar{c}(0)}. \tag{37}$$

Both ionic masses in QE-EDL and its outer edge location $x_{\min}$ computed numerically and evaluated analytically for the underlimiting current regime through Eqs. (34)–(37) are plotted in Fig. 5 versus the current density j^+ together with a

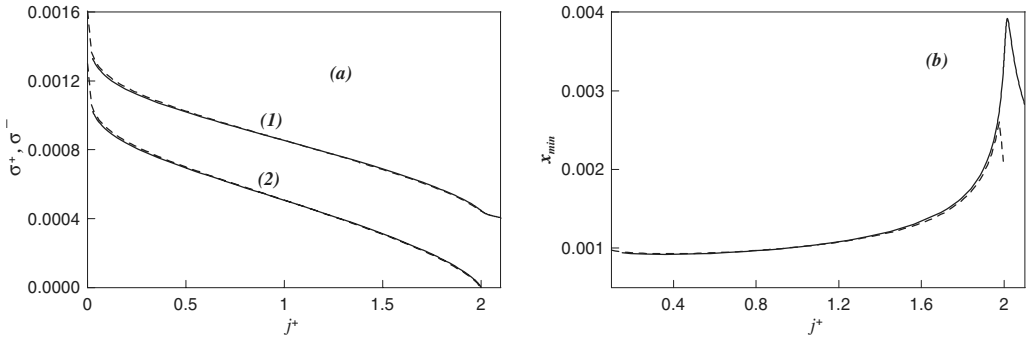

FIG. 5. (a) The EDL ionic masses σ^+ (curves 1) and σ^- (curves 2), calculated numerically for all regimes (continuous lines) and analytically for underlimiting current regime (dashed lines) versus the current density j^+; $p_1=10$, $\varepsilon=0.0001$; (b) dependence of the QE-EDL edge location, $x_{\min}$ calculated numerically for all regimes (continuous line) and analytically for underlimiting current regime (dashed line) on the current density j^+; $p_1=10$, $\varepsilon=0.0001$.

dependence of the QE-EDL edge location, $x_{\min}$, on j^+. We point out the monotonic decrease in the ionic masses and the change in direction of propagation of $x_{\min}$ near the limiting current occurred near the transitional regime $[\bar{c}(0)=O(\varepsilon^{2/3})$, $x_0=O(\varepsilon^{2/3})$, see Eq. (34)].

Let us complement the above rigorous analysis of EDL and ESC with some heuristic scaling arguments. We begin with inferring the origin of the $\varepsilon^{2/3}$ length scale.

Let us consider the ESC Region, where concentration of coions vanishes and concentration of counterions is low and nearly constant [see curves (3–5) in Fig. 3(b)]. Neglecting the diffusional cation flux component compared to the migrational one in Eqs. (1) and the anions' concentration compared to that of cations in Eq. (3), yield

$$c^+\varphi_x = j^+, \quad x_{\min} < x < x_0, \tag{38}$$

$$\varepsilon^2\varphi_{xx} = -c^+, \quad x_{\min} < x < x_0. \tag{39}$$

To evaluate the ESC layer width $x_0-x_{\min}$, we rewrite Eqs. (38) and (39) as follows:

$$\varepsilon^2\frac{d^2\varphi}{dx^2}\frac{d\varphi}{dx} \approx -j^+, \quad x_{\min} < x < x_0. \tag{40}$$

Integration of Eq. (40) yields

$$x_0 - x_{\min} \approx \frac{1}{2}\{3\varepsilon[\varphi(x_0)-\varphi(x_{\min})]\}^{2/3}(j^+)^{-1/3}. \tag{41}$$

Equation (41) implies domination of the ESC layer by the $\varepsilon^{2/3}$ length scale for the transitional range of potential drops across this layer, $O(1)\le\varphi(x)|_{x_0}^{x_{\min}}\le O(\ln\varepsilon)$, whereas for higher potential drops, $\varphi(x)|_{x_0}^{x_{\min}}=O(\varepsilon^{-\alpha})$, $0<\alpha<1$, a whole range of length scales appears, $x_0-x_{\min}=O(\varepsilon^{2/3(1-\alpha)})$, up to an ESC region of a finite size, $x_0-x_{\min}=O(1)$, for extremely high potential drops of the order of $\varphi(x)|_{x_0}^{x_{\min}}=O(\frac{1}{\varepsilon})$.

The response of QE-EDL to the formation of ESC may be traced through the force balance on the charge carriers. Integration of the Poisson Eq. (3) multiplied by φ_x, yields, taking into account Eqs. (1) and (2) and integrating the obtained expression

$$\frac{\varepsilon^2}{2}(\varphi_x^2(0)-\varphi_x^2(x_{\min}))-(p_1-c^+(x_{\min})) = j^+x_{\min},$$
$$0 < x < x_{\min}. \tag{42}$$

Equation (42) expresses the balance of forces acting on the ions in the QE-EDL; that is, balance of the drop of total pressure (sum of the Maxwell and osmotic pressures of ions in QE-EDL) with the total friction force of this charges against the water measured by $j^+x_{\min}$.

In terms of charge distribution the last equality reads

$$\Sigma_{\text{total}} \approx \sqrt{\Sigma_{\text{ESC}}^2 + 2\varepsilon^2(p_1-c^+(x_{\min}))} \approx \varepsilon\sqrt{2p_1} + \frac{\Sigma_{\text{ESC}}^2}{\varepsilon\sqrt{2p_1}} < \Sigma_{\text{ESC}} + \varepsilon\sqrt{2p_1}. \tag{43}$$

Thus, indeed, the total charge in the diffusion layer is smaller than the sum of the maximal charge of QE-EDL and the ESC, that is, the latter is formed, at least partly, at the expense of the former. Here the magnitude of ESC charge, Σ_{ESC}, is determined by Eq. (23) (valid as previously mentioned for all relevant regimes) as

$$\Sigma_{\text{ESC}} = \varepsilon\sqrt{2x_0j^+c_{\min}}. \tag{44}$$

Integration of Eq. (40) yields, taking in account Eq. (41),

$$\Sigma_{\text{ESC}} \approx \varepsilon\sqrt{2j^+(x_0-x_{\min})} \approx \varepsilon^{4/3}\{3j^+[\varphi(x_0)-\varphi(x_{\min})]\}^{1/3}. \tag{45}$$

Thus, recapitulating the entire picture, the ESC zone develops as an extension of the cation minimum formed in the course of the concentration polarization. The positive charge of ESC is formed as a result of expulsion of anions by the electric field into the locally electroneutral bulk, in which the influx of the negative charge from ESC is compensated by the influx of additional cations supplied by the anode. Simultaneously, with the formation of ESC the QE-EDL at the membrane–solution interface adjusts itself by "squeezing" a certain amount of cations back into the membrane (and then to the far cathode) so that the total charge in the solution stays almost constant and, thus, lower than the maximal charge of QE-EDL plus the ESC in accord with Eq. (43).

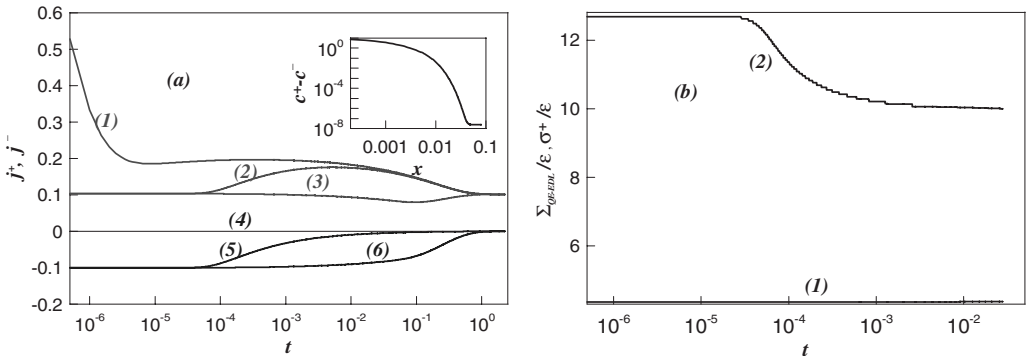

FIG. 6. (a) Ionic fluxes j^+, j^- versus time plots calculated for $\varepsilon=0.003$, $p_1=10$, $V=\ln(p_1)$, $\delta=0.1$ at: j^+: curve 1, $x=0$, curve 2, $x=x_{\min}$, curve 3, $x=1$; j^-: curve 4, $x=0$; curve 5, $x=x_{\min}$, curve 6, $x=1$. Inset to Fig. 6(a): charge-density plot versus variable x. (b) The QE-EDL charge (curve 1) and cations' QE-EDL Mass (curve 2) versus time calculated for $\varepsilon=0.003$, $p_1=10$, $V=\ln(p_1)$, $\delta=0.1$.

So far this qualitative picture was inferred from steady-state arguments. These latter maybe complemented by observations of the systems time dependent response to an instantaneous voltage increment. Let us consider the following time-dependent version of the boundary value problem [Eqs. (1)–(6)] to be analyzed with a purpose to trace the system response to an instantaneous voltage increment δ;

$$c_t^+ = \frac{\partial j^+}{\partial x}, \tag{46}$$

$$c_t^- = \frac{\partial j^-}{\partial x}, \tag{47}$$

$$\varepsilon^2 \varphi_{xx} = c^- - c^+, \tag{48}$$

$$\varphi(0,t) = -(V+\delta), \quad \varphi(1,t) = 0, \tag{49}$$

$$c^+(0,t) = p_1, \tag{50}$$

$$c^-(1,t) = 1, \quad c^+(1,t) = 1, \tag{51}$$

$$c^+(x,0) = c_0^+(x), \quad c^-(x,0) = c_0^-(x). \tag{52}$$

Here, the ionic fluxes j^+, j^- are defined by Eqs. (1) and (2), and $c_0^+(x)$, $c_0^-(x)$ are the steady-state ionic concentrations for unperturbed voltage V, t is the dimensionless time (normalized by the macroscopic diffusion time $T=L^2/D$, where D is a typical ionic diffusivity in the electrolyte solution, assumed equal for ions of both signs). The following comparison of instantaneous ionic fluxes j^+, j^- computed at key locations such as membrane/solution interface $x=0$, right edge of the QE-EDL $x_{\min}$, and diffusion layer/stirred bulk interface $x=1$ stands in line with the above scenario of ESC formation.

Thus, in Fig. 6(a) we present the time dependence of fluxes computed near the equilibrium at the aforementioned key locations. Comparing the cationic j^+ flux (curve 1) calculated at the membrane/solution interface, $x=0$, and at the right edge of the QE-EDL (curve 2), $x=x_{\min}$, we observe a decrease in the total cations' mass [curve 2, Fig. 6(b)] in QE-EDL. Simultaneously, an almost identical decrease in anionic mass due to the anions expulsion from QE-EDL [curve 5, Fig. 6(a)] preserves the QE-EDL charge nearly constant.

In Figs. 7(a) and 7(b) we present similar plots computed for the perturbation of a transitional state from quasiequilibrium to nonequilibrium, $V=\ln(p_1)+10$. We note a decrease in anionic concentration in QE-EDL with voltage which yields curves 1 (total QE-EDL charge) and 2 (total cation's QE-EDL Mass) approaching each other in Fig. 7(b).

Finally, in Fig. 8 we present the corresponding plots for perturbation of a strongly nonequilibrium state, $V=\ln p_1 + 20$. We note vanishing of the anionic concentration in EDL

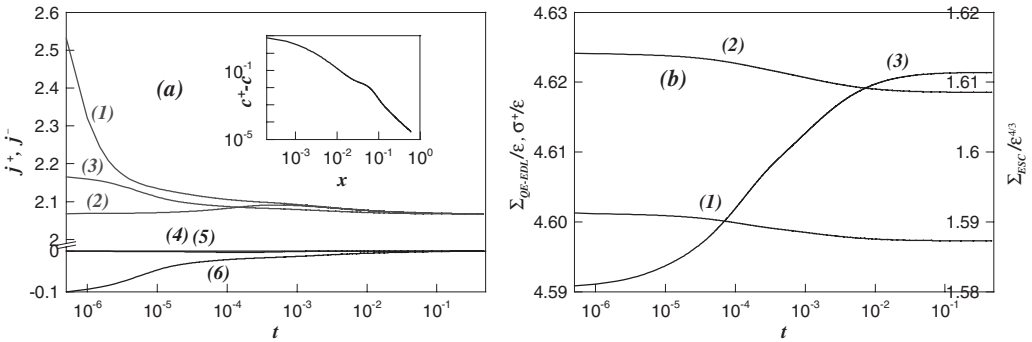

FIG. 7. (a) Ionic fluxes j^+, j^- versus time plots calculated for $\varepsilon=0.003$, $p_1=10$, $V=\ln(p_1)+10$, $\delta=0.1$ at j^+: curve 1, $x=0$; curve 2, $x=x_{\min}$, curve 3, $x=1$; j^-: curve 4, $x=0$; curve 5, $x=x_{\min}$; and curve 6, $x=1$. Inset to Fig. 7(a): steady-state charge-density plot versus variable x. (b) The QE-EDL charge (curve 1), cations' QE-EDL Mass (curve 2), and ESC charge (curve 3) versus time calculated for $\varepsilon=0.003$, $p_1=10$, $V=\ln(p_1)+10$, $\delta=0.1$.

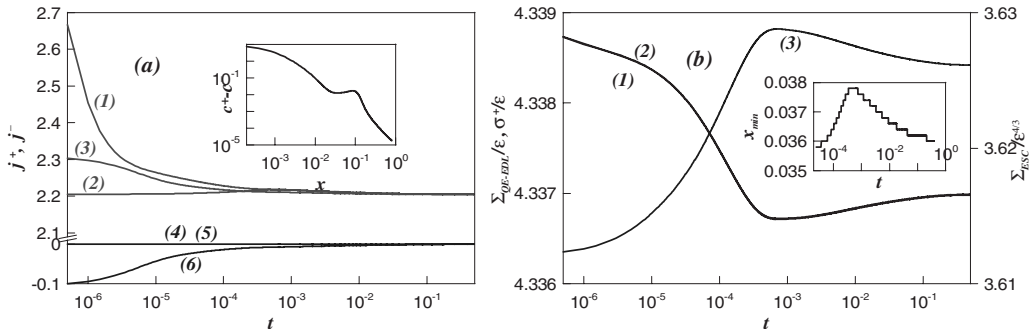

FIG. 8. (a) Ionic fluxes j^+, j^- versus time calculated for $\varepsilon=0.003$, $p_1=10$, $V=\ln(p_1)+20$, $\delta=0.1$ at: j^+: curve 1, $x=0$; curve 2, $x=x_{\min}$, curve 3, $x=1$; j^-: curve 4, $x=0$; curve 5, $x=x_{\min}$; and curve 6, $x=1$. Inset to Fig. 8(a): charge density versus x. (b) The QE-EDL charge (curve 1), QE-EDL cations' Mass (curve 2), and ESC charge (curve 3) versus time calculated for $\varepsilon=0.003$, $p_1=10$, $V=\ln(p_1)+20$, $\delta=0.1$. Inset to Fig. 8(b): QE-EDL right edge location $x_{\min}$ versus time t.

accompanied by merging of the curves 1 (total QE-EDL charge) and 2 (total mass of cations in QE-EDL) in Fig. 8(b). We also note a slight nonmonotonicity of the curves 1–3 [Fig. 8(b)] resulting from a slight nonmonotonic shift of the location of the right edge of QE-EDL [inset to Fig. 8(b)].

Thus summarizing, the presented picture of temporal response indeed confirms the view of development of ESC zone as an extension of the cations' minimum neighborhood. The positive charge of ESC is formed as a result of the expulsion of anions by the electric field into the locally electroneutral bulk, where the influx of the negative charge is compensated by that of additional cations from the anode. Simultaneously, with the formation of ESC, the QE-EDL at the membrane-solution interface adjusts itself by "squeezing" a certain amount of cations back into the membrane (and then further on to the cathode) so that the total charge in the solution remains nearly constant or, rather, lower than the sum of the maximal charge of QE-EDL and the ESC, in accord with Eq. (43). We also note that for all regimes of EDL, the charge variation in QE-EDL under increase in the applied electric field occurs through a suitable decrease in the total amount of ions of both signs: counterions leave the solution through the depleted interface, whereas coions are expelled from the diffusion layer into the bulk and further on to the anode.

We conclude this section with singling out the main peculiarity of ESC compared to the QE-EDL charge, underlying its related macroscopic effects, such as nonequilibrium electro-osmotic instability [19] and AR [2]. According to Eq. (21), the QE-EDL charge depends only on the electro-neutral interface concentration, with the potential drop across the layer related to the former by the Donnan's equation. As opposed to this, the ESC depends on both the potential drop across the EDL (ζ potential) and the interface value of the electro-neutral ionic concentration gradient [see Eq. (45)]. For an ideally permselective interface, the former is proportional to the electric current density. In the general case, it is proportional to the "salt flux," defined in the next section. This difference in the control parameters of the QE-EDL and ESC determines the difference of the system's response to external perturbations. Thus, in the underlimiting regime, the QE-EDL charge and its related charge density decrease upon the increase in the interface solute concentration. On the other hand, at the limiting current, an increase in the interface concentration gradient (parallel to the increase in the interface concentration in the underlimiting regime since the former is very low) yields contraction of the width of the ESC region, with the total ESC charge practically unchanged, that is yields an increase in the charge density. Namely this difference in response underlies both nonequilibrium electro-osmotic instability and AR.

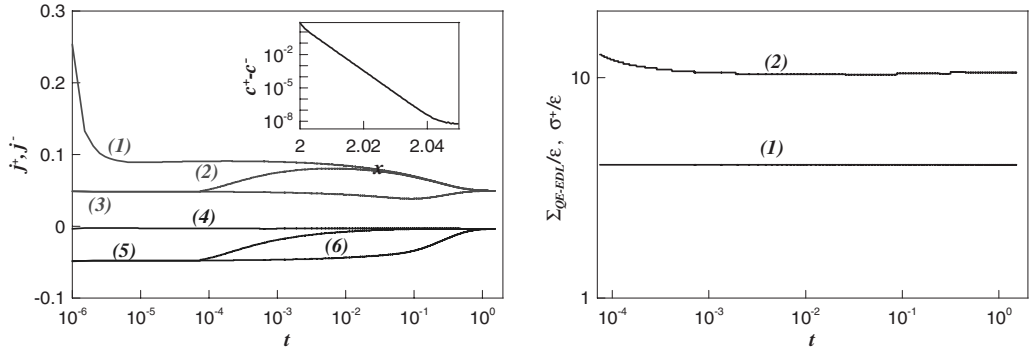

FIG. 9. Three-layer model for a highly charged membrane: $N=10e$; (a) the ionic fluxes j^+, j^- versus time calculated for $\varepsilon=0.003$, $V=0$, $\delta=0.1$, $D=1$ at j^+: curve 1, $x=0$; curve 2, $x=x_{\min}$, curve 3, $x=1$; j^-: curve 4, $x=0$; curve 5, $x=x_{\min}$; and curve 6, $x=1$. Inset to Fig. 6(a): charge-density plot versus variable x. (b) The QE-EDL charge (curve 1) and cations' QE-EDL Mass (curve 2) versus time calculated for $\varepsilon=0.003$, $V=0$, $\delta=0.1$, $D=1$.

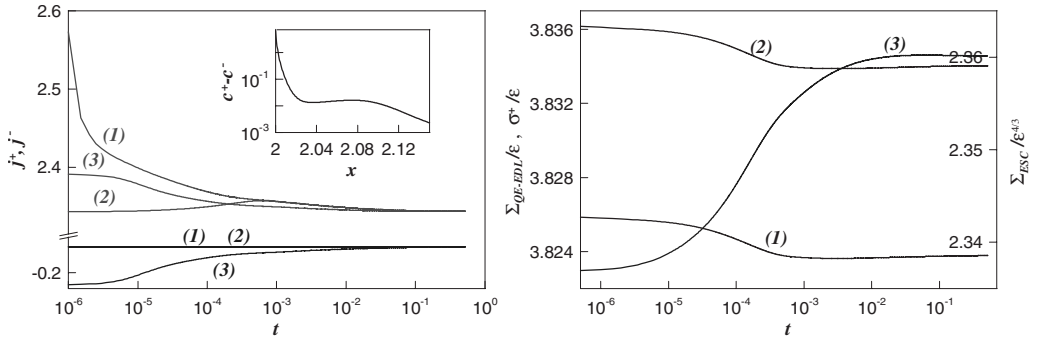

FIG. 10. Three-layer model for a highly charged membrane: $N=10e$; (a) the ionic fluxes j^+, j^- versus time calculated for $\varepsilon=0.003$, $V=20$, $\delta=0.1$, $D=1$ at j^+: curve 1, $x=0$; curve 2, $x=x_{\min}$, curve 3, $x=1$; j^-: curve 4, $x=0$; curve 5, $x=x_{\min}$; and curve 6, $x=1$. Inset to Fig. 6(a): charge-density plot versus variable x. (b) The QE-EDL charge (curve 1), cations' QE-EDL Mass (curve 2), and ESC charge (curve 3) versus time calculated for $\varepsilon=0.003$, $V=20$, $\delta=0.1$, $D=1$.

IV. THREE-LAYER MODEL

To test the universality of the above one-layer scenario, let us consider a three layer problem concerning a nonideal cation-exchange membrane, $1<x<2$, separating two electrolyte diffusion layers, $0<x<1$ and $2<x<3$, flanked on the outside by two stirred bulks. The corresponding 1D time-dependent formulation reads

$$c_t^+ = j_x^+, \quad 0<x<3, \quad t>0, \tag{53}$$

$$c_t^- = j_x^-, \quad 0<x<3, \quad t>0, \tag{54}$$

$$\varepsilon^2 \varphi_{xx} = Q(x) + c^- - c^+, \quad Q(x) = N[H(x-1) - H(x-2)], \quad 0<x<3, \quad t>0, \tag{55}$$

$$\varphi(0,t) = -V-\delta, \quad \varphi(3,t)=0, \quad c^+(0,t) = c^-(0,t) = c^+(3,t) = c^-(3,t) = 1, \tag{56}$$

$$c^+(x,0) = c_0^+(x), \quad c^-(x,0) = c_0^-(x). \tag{57}$$

The dimensionless ionic fluxes are given by Eqs. (1) and (2), δ is the instantaneous voltage perturbation, $c_0^{\pm}$ are the respective unperturbed steady-state ionic concentrations, corresponding to the unperturbed voltage V. Unity dimensionless ionic diffusivities in the electrolyte and in the membrane are assumed for simplicity, in order to focus entirely on the electrostatics of EDL and concentration polarization. Generalization of the subsequent analysis to a more realistic situation is straightforward.

We begin with consideration of a highly charged cation selective membrane ($N \gg 1$). In Figs. 9(a) and 10(a) we present the time-dependence of the ionic fluxes at the membrane/solution interface, $x=0$, at the right edge of the QE-EDL, $x=x_{\min}$ and at the depleted diffusion layer/stirred bulk interface, $x=1$, for a perturbation near the equilibrium ($V=0$) and away from it ($V=20$). Furthermore, in Figs. 9(b) and 10(b), we present the time dependence of the QE-EDL charge, the total mass of cations and ESC showing a close agreement between the one- and three-layer models for a highly charged membrane ($N=10e$).

The corresponding results for a moderately charged membrane $N=O(1)$ are presented in Figs. 11 and 12. Thus, in Fig. 11(a) we present the time dependence of the ionic fluxes at the membrane/solution interface, $x=0$, at the right edge of the QE-EDL (curve 2), $x=x_{\min}$ and at the depleted diffusion layer/stirred bulk interface, $x=x_{\min}$ for a perturbation near the equilibrium ($V=0$) state for $N=e$. For short times, for this kind of membrane the charge of EDL increases near the equilibrium due to both expulsion of anions by the electric field and diffusion driven exit of additional cations from the membrane. For longer times, the cation flux reverses its sign [see curve 1, Fig. 11(a)] with the cations driven back to the mem-

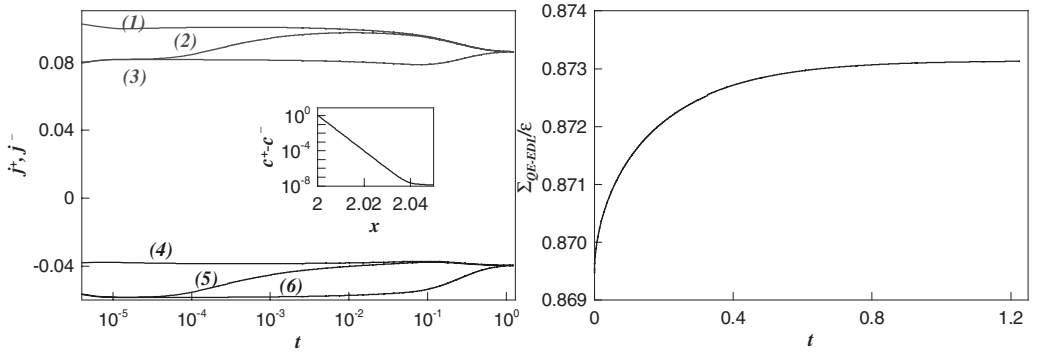

FIG. 11. Three-layer model for a moderately membrane: $N=e$; (a) the ionic fluxes j^+, j^- versus time calculated for $\varepsilon=0.003$, $V=0.1$, $\delta=0.1$, $D=1$ at j^+: curve 1, $x=0$; curve 2, $x=x_{\min}$, curve 3, $x=1$; j^-: curve 4, $x=0$; curve 5, $x=x_{\min}$; and curve 6, $x=1$. Inset to Fig. 6(a): charge-density plot versus variable x. (b) The QE-EDL charge $\varepsilon=0.003$, $V=0$, $\delta=0.1$, $D=1$.

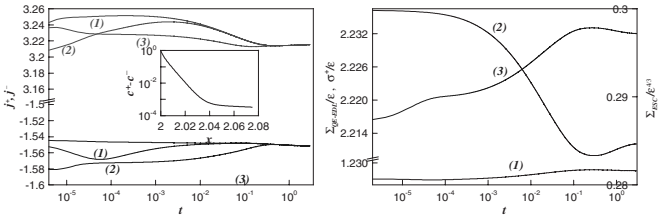

FIG. 12. Three-layer model for a moderately charged membrane: $N=e$; (a) the ionic fluxes j^+, j^- versus time calculated for $\varepsilon=0.003$, $V=30$, $\delta=0.1$, $D=1$ at: j^+: curve 1, $x=0$; curve 2, $x=x_{\min}$, curve 3, $x=1$; j^-: curve 4, $x=0$; curve 5, $x=x_{\min}$; and curve 6, $x=1$. Inset to Fig. 6(a): charge-density plot versus variable x. (b) The QE-EDL charge (curve 1), cations' QE-EDL Mass (curve 2), and ESC charge (curve 3) versus time calculated for $\varepsilon=0.003$, $V=30$, $\delta=0.1$, $D=1$.

brane by the electric field. In Fig. 11(b) we present the corresponding time dependence of the QE-EDL charge.

Finally, in Fig. 12 we present similar plots for a nonequilibrium regime. We note the nonmonotonicity of the QE-EDL charge and QE-EDL's cations' mass in these plots and the presence of a significant number of anions in the QE-EDL in the high-voltage regime for a low selectivity membrane.

V. REDUCTION IN THE THREE-LAYER MODEL TO ONE-LAYER

In order to analyze the effect of membrane selectivity on the dynamics of QE-EDL and ESC adjacent to the depleted membrane/solution interface, below we reduce the three-layer model [Eqs. (53)–(57)] to a much simpler one-layer setup. Let us consider the following steady-state version of the problem [Eqs. (53)–(57)]:

$$\overset{\text{def}}{j^+ = D(x)(c_x^+ + c^+\varphi_x) = \text{const}}, \quad 0 < x < 3 \tag{58}$$

$$\overset{\text{def}}{j^- = D(x)(c_x^- - c^-\varphi_x) = \text{const}}, \quad 0 < x < 3 \tag{59}$$

$$\varepsilon^2\varphi_{xx} = Q(x) + c^- - c^+, \quad 0 < x < 3, \tag{60}$$

$$\varphi(0) = -V, \quad \varphi(3) = 0, \quad c^+(0) = c^-(0) = c^+(3) = c^-(3) = 1. \tag{61}$$

Here

$$\overset{\text{def}}{Q(x) = N[H(x-1) - H(x-2)]} \tag{62}$$

is the fixed charge density (0 in the electrolyte layers and $N>0$ in the membrane) and

$$\overset{\text{def}}{D(x) = 1 + (D-1)[H(x-1) - H(x-2)]}, \tag{63}$$

where D is the dimensionless ionic diffusivity in the membrane assumed equal for both types of ions, compared to their unity diffusivity in solution.

A. Solution of the "outer" problem

We begin the analysis of problem [Eqs. (58)–(63)] with consideration of the "outer" QEB problem. The "outer" unknowns are the bulk electric potential $\tilde{\varphi}$ and bulk ionic concentration c:

$$\overset{\text{def}}{c = c^{\pm} \mp \frac{Q(x)}{2}} = \begin{cases} c^+ = c^-, & 0 < x < 1- \quad \text{or} \quad 2+ < x < 3, \\ c^+ - \dfrac{N}{2} = c^- + \dfrac{N}{2}, & 1+ < x < 2-. \end{cases} \tag{64}$$

Integration of Eqs. (58) and (59) in the electroneutral part of the solution yields

$$c = \begin{cases} \dfrac{J}{2}x + 1, & 0 < x < 1 \\ \dfrac{J}{2}(x-3) + 1, & 2 < x < 3, \end{cases} \tag{65}$$

$$\tilde{\varphi} = \begin{cases} \dfrac{I}{J}\ln\left(\dfrac{J}{2}x + 1\right) - V, & 0 < x < 1 \\ \dfrac{I}{J}\ln\left(\dfrac{J}{2}(x-3) + 1\right), & 2 < x < 3, \end{cases} \tag{66}$$

with the unknown constant "salt flux" J and electric current I, defined as

$$\overset{\text{def}}{J = j^+ + j^- = 2c_x}, \tag{67}$$

$$\overset{\text{def}}{I = j^+ - j^- = 2c\tilde{\varphi}_x}. \tag{68}$$

Taking into account continuity of electrochemical potentials yields the following boundary-value problem for the electroneutral portion of the membrane:

$$c_x + \frac{N}{2}\tilde{\varphi}_x = \frac{J}{2D}, \quad 2 < x < 3, \tag{69}$$

$$c\tilde{\varphi}_x = \frac{I}{2D}, \quad 2 < x < 3, \tag{70}$$

$$c(1+) = \sqrt{\frac{N^2}{4} + \left(\frac{J}{2} + 1\right)^2}, \tag{71}$$

$$\tilde{\varphi}(1+) = \left(\frac{I}{J} + 1\right)\ln\left(\frac{J}{2} + 1\right) - V - \ln\left[\sqrt{\frac{N^2}{4} + \left(\frac{J}{2} + 1\right)^2} + \frac{N}{2}\right], \tag{72}$$

$$c(2-) = \sqrt{\frac{N^2}{4} + \max\left[\left(1 - \frac{J}{2}\right), 0\right]^2}, \tag{73}$$

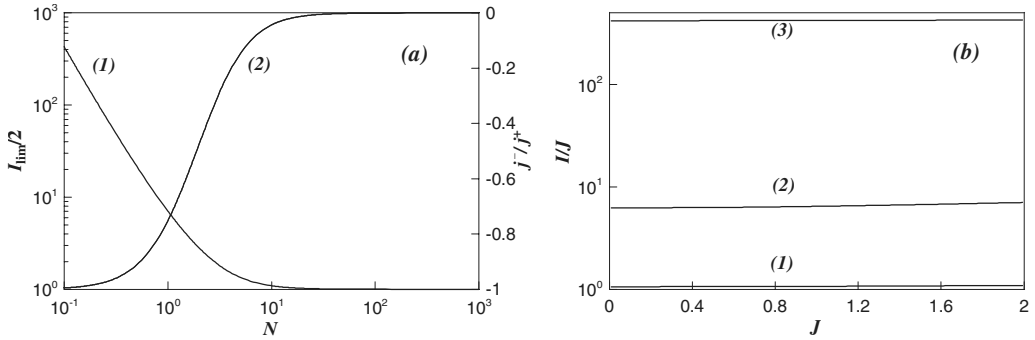

FIG. 13. (a) Curve 1: dependence of the half limiting electric current I_{lim} (the ratio of the limiting current and the limiting salt flux $J=2$) on the fixed charge density N in the three-layer model, for a fixed membrane resistance $R=1$; curve 2: dependence of the limiting fluxes ratio $\lim_{V\to\infty}\frac{j^-}{j^+}$ on the fixed charge density N in the three-layer model for a fixed membrane resistance $R=1$; (b) The dependence of electric/salt flux ratio, $\frac{I}{J}$, on salt flux J for $N=10$ (curve 1), $N=1$ (curve 2), $N=0.1$ (curve 3), and $R=1$.

$$\tilde{\varphi}(2-)=\left(\frac{I}{J}+1\right)\ln\left(1-\frac{J}{2}\right)-\ln\left[\sqrt{\frac{N^2}{4}+\left(1-\frac{J}{2}\right)^2}+\frac{N}{2}\right]. \tag{74}$$

The formulation [Eqs. (69)–(74)] is valid for all regimes, except for the boundary condition [Eq. (74)] which fails along with continuity of electrochemical potentials across the depleted interface at the limiting current, when $J\to 2$.

Substituting Eq. (70) into Eq. (71) and integrating the resulting equation, we find

$$\frac{c}{J}+\frac{IN}{2J^2}\ln\left(\frac{IN}{2J}-c\right)=\frac{x}{2D}+\text{const}. \tag{75}$$

Substitution of boundary conditions [Eqs. (71) and (73)] into Eq. (75) yields

$$\frac{-8}{\sqrt{N^2+(2-J)^2}+\sqrt{N^2+(2+J)^2}}+\frac{IN}{J^2}\ln\frac{\frac{IN}{J}-\sqrt{N^2+(2-J)^2}}{\frac{IN}{J}-\sqrt{N^2+(2+J)^2}}$$

$$=\frac{1}{D}. \tag{76}$$

Equation (76), valid for all regimes, determines the dependence of the electric current I on J. For the large fixed charge limit $N\gg 1$, Eq. (76) yields to the leading order

$$\frac{J}{I}=1+\frac{1}{R}O\left(\frac{1}{N^2}\right). \tag{77}$$

Here

$$R\overset{\text{def}}{=}\frac{1}{DN} \tag{78}$$

is membrane resistance which we assume to be of the order unity. Thus, as expected the limit of high membrane's charging, implies ideal permselectivity, with coions flux vanishing and the salt flux and the electric current coinciding:

$$j^-=\frac{1}{R}O\left(\frac{1}{N^2}\right), \tag{79}$$

Taking, the limiting current limit, $J\to 2$, in Eq. (76) we find

$$\frac{I_{lim}N}{4}\ln\frac{I_{lim}N-2N}{I_{lim}N-2\sqrt{N^2+16}}-\frac{8}{N+\sqrt{N^2+16}}=\frac{1}{D}. \tag{80}$$

In Fig. 13(a) we present the dependence of the limiting electric current I_{lim} on the fixed charge density N for a fixed membrane resistance. In Fig. 13(b) we present the dependence of the ratio of the salt flux versus electric current on the salt flux J for the three cases of a slightly charged ($N=0.1$), moderately charged ($N=1$), and highly charged membrane ($N=10$). We note the low sensitivity of this ratio to the salt flux and, correspondingly, to the applied voltage. We also note that Eq. (76) and, correspondingly, the dependence presented in Fig. 13, are valid for all voltage regimes.

B. Solution of the "inner" problem

Below we solve the problem [Eqs. (58)–(63)] in the membrane QE-EDL and, using the solution to the outer problem obtained above, reduce the three-layer model to a one-layer formulation valid for a nonideal ion-selective membrane.

Solution of Eqs. (58) and (59) in the membrane QE-EDL, $2-O(\varepsilon)\le x<2$, yields the following Boltzmann relations for the ionic concentrations:

$$c^+=\left(c(2-)+\frac{N}{2}\right)e^{\tilde{\varphi}(2-)-\varphi(x)},\quad c^-=\left(c(2-)-\frac{N}{2}\right)e^{\varphi(x)-\tilde{\varphi}(2-)}. \tag{81}$$

Here $c(2-)$, $\tilde{\varphi}(2-)$ are, respectively, the membrane/solution interface values of the outer ionic concentration and electric potential at the membrane's side [see Eq. (64)]. Note that an analogous integration across the EDL at the depleted electrolyte side of the membrane/solution interface is valid only for underlimiting regime.

Multiplying the Poisson Eq. (60) by φ', substituting Eqs. (58) and (59), and integrating the obtained equation across the QE-EDls, we obtain the following expressions for the inner electric field, analogous to Eq. (42) and bearing the same physical meaning

$$\varepsilon^2\varphi'^2|_{2-}^{x} = 2\{N[\varphi(x)-\tilde{\varphi}]+c^+ + c^- - 2c(2-) + J\cdot O(\varepsilon)\},$$
$$2 - O(\varepsilon) \le x \le 2, \tag{82}$$

$$\varepsilon^2\varphi'^2|_{2+}^{x} = 2[c^+ + c^- - 2c(2+) + J\cdot O(\varepsilon)],$$
$$2 \le x \le 2 + O(\varepsilon). \tag{83}$$

For the membrane/solution interface, $x=2$, the latter two equations yield

$$N(\varphi(2)-\tilde{\varphi}(2-)) + 2c(2+) - 2c(2-) = 0. \tag{84}$$

Taking into account Eqs. (74), we find the potential drop across the membrane QE-EDL:

$$\varphi(2)-\tilde{\varphi}(2-) = \sqrt{1+\left(\frac{2c(2+)}{N}\right)^2} - \frac{2c(2+)}{N} = 1 + O\left(\frac{c(2+)}{N}\right). \tag{85}$$

Substitution of this expression into the Boltzmann relation (84) yields

$$c^+(2) = \left[\sqrt{\frac{N^2}{4}+c(2+)^2}+\frac{N}{2}\right]e^{[2c(2+)/N]-\sqrt{1+[2c(2+)/N]^2}} = \frac{N}{e}\left\{1+O\left[\frac{c(2+)}{N}\right]\right\}. \tag{86}$$

Thus, we are able to evaluate the interface cation concentration in terms of fixed charge density N and the outer EN bulk interface concentration, $c(2+)=1-\frac{J}{2}$, only. We note that for the limiting current regime, $J\approx 2$, or high fixed charge density, $N\gg 1$, Eqs. (85) and (86) yield

$$\varphi(2)-\tilde{\varphi}(2-)=1, \quad c^+(2)=\frac{N}{e}. \tag{87}$$

The last equation justifies the determination of the interface cation's concentration in the one-layer problem [Eqs. (1)–(6)]. Thus, the maximal potential drop across membrane QE-EDL is independent of the fixed charge density and equal to unity or thermal potential in terms of dimensional variables. Since, according to Eq. (76), flux ratio depends only on the fixed charge density N and, the salt flux J, that is the voltage V (recall the virtual independence of this ratio of the voltage) to complete the formulation we have to find the potential drop across the electrolyte layer in terms of the voltage V.

To this end, we integrate Eq. (69) across the electroneutral portion of the membrane and use the boundary conditions at the enriched electrolyte layer/membrane interface, $x=1$, where continuity of electrochemical potentials is valid for all regimes. This integration yields

$$c(2-)-c(1+)+\frac{N}{2}[\tilde{\varphi}(2-)-\tilde{\varphi}(1+)] = \frac{J}{2D} \tag{88}$$

and

$$\tilde{\varphi}(2-) = \sqrt{1+\left(\frac{2+J}{N}\right)^2} - \sqrt{1+\left[\max\left(\frac{2-J}{N},0\right)\right]^2} + \left(\frac{I}{J}+1\right)\ln\left(\frac{J}{2}+1\right) - V - \ln\left[\sqrt{\frac{N^2}{4}+\left(\frac{J}{2}+1\right)^2} + \frac{N}{2} + \frac{J}{2DN}\right]. \tag{89}$$

Finally, referring to the flux ratio $G(N,J)\overset{\text{def}}{=}\frac{I}{J}$ determined by Eqs. (76) and (89), we complete the formulation of the model problem for the depleted diffusion layer of the three-layer setup:

$$c_x^+ + c^+\varphi_x = \frac{1+G(N,J)}{2}J, \quad 2<x<3, \tag{90}$$

$$c_x^- - c^-\varphi_x = \frac{1-G(N,J)}{2}J, \quad 2<x<3, \tag{91}$$

$$\varepsilon^2\varphi_{xx} = c^- - c^+, \quad 2<x<3, \tag{92}$$

$$c^-(3)=1, \quad c^+(3)=1, \quad \varphi(3)=0, \tag{93}$$

$$c^+(2) = \frac{1}{2}(\sqrt{N^2+[\max(2-J,0)]^2}+N)e^{(2-J/N)-\sqrt{1+(2-J/N)^2}}, \tag{94}$$

$$\varphi(2) = \sqrt{1+\left(\frac{2+J}{N}\right)^2} + [G(N,J)+1]\ln\left(\frac{J}{2}+1\right) - V - \ln\left[\sqrt{\frac{N^2}{4}+\left(\frac{J}{2}+1\right)^2}+\frac{N}{2}\right] - \max\left(\frac{2-J}{N},0\right) + \frac{J}{2DN}. \tag{95}$$

Let us recall that for the high-voltage regime or high fixed charge density, boundary condition [Eq. (94)] is simplified to $c^+(2)=\frac{N}{e}$.

C. EDL charge dynamics in the nonideal one-layer setup under current

In the remainder of this section we reproduce the analysis of Secs. II and III for the nonideal one-layer formulation [Eqs. (90)–(95)]. We rewrite the unscaled Painleve Eq. (13) as

$$\varepsilon^2\frac{d^2E}{dy^2} = \frac{1}{2}E^3 + J(x-x_0)E + G(N,J)J\varepsilon \tag{96}$$

and redefine the boundary layer variables F and z, Eq. (14) via equalities

$$E = [G(N,J)J]^{1/3}\varepsilon^{1/3}F, \quad y = [G(N,J)J]^{-1/3}\varepsilon^{2/3}z. \tag{97}$$

In terms of these variables, the boundary value problem [Eqs. (90)–(95)] is transformed into

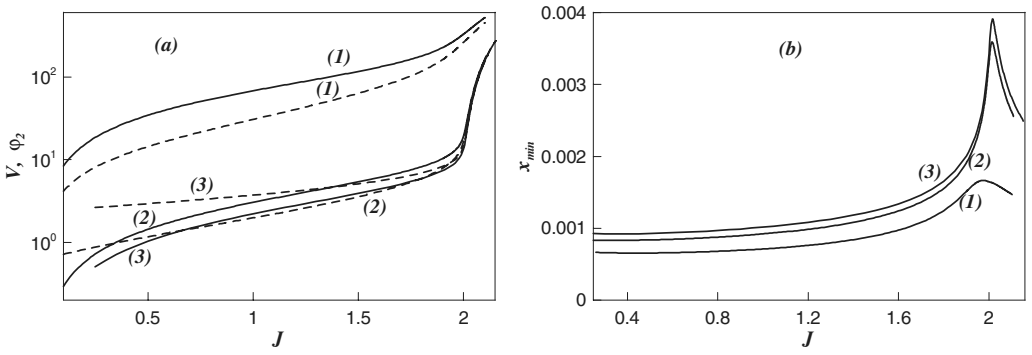

FIG. 14. (a) Dependence of the total potential drop V (continuous line) and the potential drop across the depleted electrolyte layer $-\varphi_2$ (dashed line) on the diffusional current J for three values of membranes' fixed charge $N=\frac{e}{10}$ (curves 1), $N=e$ (curves 2), $N=10e$ curves (3), and $R=1$; (b) dependence of the QE-EDL thickness $x_{\min}$ on the diffusional current J for three values of membranes' fixed charge $N=\frac{e}{10}$ (curves 1), $N=e$ (curves 2), $N=10e$ curves (3), and $R=1$.

$$\frac{d^2F}{dz^2} = \frac{1}{2}F^3 + \frac{z-z_0}{G(N,J)}F + 1, \quad 0 < z, \tag{98}$$

$$\left(\frac{dF}{dz} + \frac{1}{2}F^2\right)\Big|_{z=0} = (G(N,J)J\varepsilon)^{-2/3}(\sqrt{N^2+(2-J)^2}+N) \times e^{(2-J/N)-\sqrt{1+(2-J/N)^2}} + \frac{z_0}{G(N,J)}, \tag{99}$$

$$F(z) = -\frac{G(N,J)}{z-z_0} \quad \text{for} \quad z \gg z_0(\text{QEB}), \tag{100}$$

$$\lim_{z\to\infty}\left[\int_0^z F(z)dz + \ln(z-z_0)\right] = -\frac{2}{3}\ln\varepsilon + \frac{1}{3}\ln G(N,J) - \frac{2}{3}\ln J + \varphi(2) + \ln 2, \tag{101}$$

where $\varphi(2)$ is given by Eq. (95) and J is determined by requiring the "outer" concentration to vanish at $x=x_0$, yielding

$$J = 2(1-[G(N,J)J]^{1/3}\varepsilon^{2/3}z_0). \tag{102}$$

Here z_0 is

$$z_0 = [G(N,J)J]^{1/3}\varepsilon^{-2/3}x_0. \tag{103}$$

In Fig. 14(a) we present the dependence of the voltage V and potential drop across the depleted electrolyte layer $-\varphi_2$ on the salt flux J for three values of the fixed charge $N=\frac{e}{10}$, $N=e$, $N=10e$. In Fig. 14(b) we present the dependence of the QE-EDL thickness $x_{\min}$ on J for the same three values of the fixed charge ($N=\frac{e}{10}$, $N=e$, $N=10e$). We note the increase in x_0 with the fixed charge and the shrinking of the QE-EDL at the limiting current.

In Fig. 15(a) we present the dependence of the ionic masses σ^+ and σ^- in the depleted QE-EDL on the salt flux J for three values of membranes' fixed charge $N=\frac{e}{10}$, $N=e$, $N=10e$. We note that both masses decrease with the increase in the J (V) for all values of fixed charge density N, whereas the anions' mass vanishes at the limiting current regime only for moderate and high values of N. In Fig. 15(b) we present the corresponding dependence of the total charge Σ_{total} in the depleted electrolyte layer $2<x<3$, and the QE-EDL charge $\Sigma_{\text{QE-EDL}}$ on J for the same three values of N. We note the linear increase in the total charge with J, that implies its saturation for high voltages [see Fig. 14(a)] and the decrease in the QE-EDL charge for high voltages.

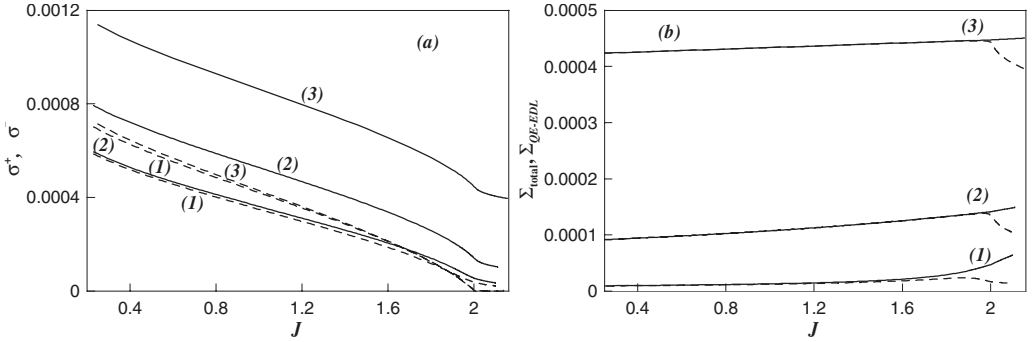

FIG. 15. (a) Dependence of cation-selective membrane/depleted electrolyte layer QE-EDL cations' σ^+ (continuous line) and anions' σ^- masses (dashed line) on the diffusional current J for three values of membranes' fixed charge $N=\frac{e}{10}$ (curves 1), $N=e$ (curves 2), $N=10e$ curves (3), and $R=1$; (b) dependence of the total depleted electrolyte layer charge $2<x<3$, Σ_{total} (continuous line), and the respective QE-EDL charge $\Sigma_{\text{QE-EDL}}$ (dashed line) on the diffusional current J $N=\frac{e}{10}$ (curves 1), $N=e$ (curves 2), $N=10e$ curves (3), and $R=1$.

VI. CONCLUSIONS

Our main conclusion in this study is that the extended space charge in concentration polarization, although always related to the quasiequilibrium electrical double layer, is not a part of it. Rather, ESC is a separate entity developing from the counterions' minimum zone, which forms in the course of CP near the depleted solid/liquid interface. Dynamics of ESC, although bearing some features common with that of QE-EDL, is different from the dynamics of the latter. In the toy model in Appendix A below both QE-EDL and ESC, absent at the equilibrium at zero current, emerge in the course of CP, with the development of the former preceding that of the latter. The summarizing sentence for the relation between the properties of ESC and its induced effects might be this: the vigor of the ESC related flows (such as Dukhin's vortices or those in the nonequilibrium electro-osmotic instability) compared to common quasiequilibrium electro-osmotic flows results from the greater distance of ESC from the wall compared to QE-EDL. The very occurrence of critical effects of ESC (such as anomalous rectification and nonequilibrium electro-osmotic instability) is due to peculiarities of ESC response to external perturbations.

ACKNOWLEDGMENT

The work was supported by the Israel Science Foundation (Grant No. 65/07).

APPENDIX A: EDL CHARGE DYNAMICS IN A TOY PROBLEM

To illustrate the particular relation between the QE-EDL and ESC let us analyze the following toy model in which anions are sterically prohibited from crossing an infinitesimally thin membrane located at $x=0$, and separating two diffusion layers $-1<x<0$, $0<x<1$, flanked on the outside by two stirred bulks. The corresponding boundary value problem reads

$$j^+ \overset{\text{def}}{=} c_x^+ + c^+\varphi_x = \text{const}, \quad -1<x<1, \tag{A1}$$

$$j^- \overset{\text{def}}{=} c_x^- - c^-\varphi_x = 0, \quad -1<x<1, \quad x\neq 0, \tag{A2}$$

$$\varepsilon^2\varphi_{xx} = c^- - c^+, \quad -1<x<1, \tag{A3}$$

$$c^-(\pm 1)=1, \quad c^+(\pm 1)=1, \quad \varphi(-1)=-V, \quad \varphi(1)=0. \tag{A4}$$

Integration of Eq. (A2) and substitution of boundary conditions [Eq. (A4)] yield

$$c^- = \begin{cases} e^{\varphi+V}, & -1<x<0 \\ e^{\varphi}, & 0<x<1. \end{cases} \tag{A5}$$

Similarly with a consideration of the three-layer problem [Eqs. (58)–(62)] we integrate the three-layer problem [Eqs. (A1)–(A5)] across the enriched electrolyte layer $-1<x<0$ and reduce it to a one-layer setup. We start integration of the respective outer "electroneutral bulk" problem with the left, enriched electrolyte layer $-1<x<0$. The respective electroneutral electrolyte concentration and electric potential read

$$c = 1+\frac{j^+}{2}(x+1), \quad \tilde{\varphi} = \ln\left(1+\frac{j^+}{2}(x+1)\right), \quad -1<x<0. \tag{A6}$$

Continuity of the cations' electrochemical potential across the QE-EDL in this enriched diffusion layer yields

$$\ln(c^+(0))+\varphi(0) = 2\ln\left(1+\frac{j^+}{2}\right)-V. \tag{A7}$$

To complete the formulation of the one-layer problem we employ the pressure balance across both EDLs similar to Eq. (42). Thus, multiplying the Poisson Eq. (A3) by φ', substituting Eqs. (A1) and (A4) and integrating the obtained equations across the electrolyte layers $-1<x<0$, $0<x<1$, we obtain the following expressions for the inner electric field at $x=0$:

$$\varepsilon^2\varphi'(0)^2 = 2(c^+(0)+e^{\varphi(0)+V})-2(2-j^+) = 2(c^+(0)+e^{\varphi(0)}) - 2(2+j^+), \tag{A8}$$

and find the potential drop across depleted electrolyte layer

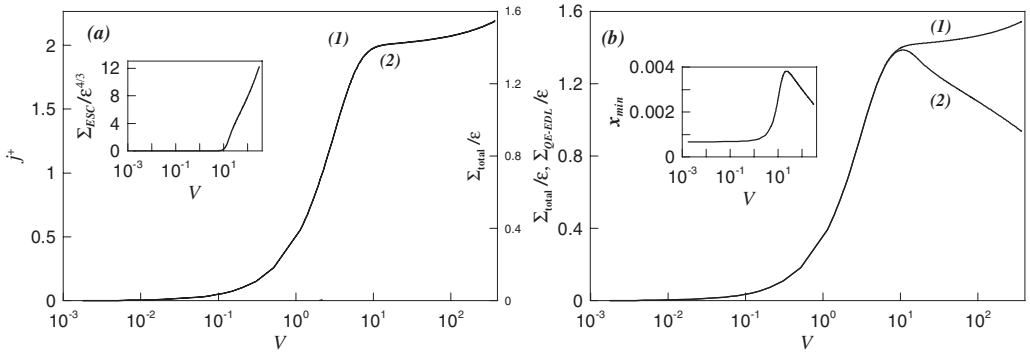

FIG. 16. (a) Voltage-current dependence (curve 1) and right (depleted) electrolyte layer's charge-voltage (curve 2) dependence for the "toy" problem. Inset to Fig. 16(a): ESC versus voltage plot; (b) right electrolyte layer charge-voltage (curve 1) and right QE-EDL–voltage dependence (curve 2) for the toy problem. Inset to Fig. 16(b): depleted electrolyte layer's QE-EDL right edge's location's dependence on the applied voltage.

$$\varphi(0) = \ln\left(-\frac{2j^+}{e^V - 1}\right). \tag{A9}$$

The latter condition completes the formulation of the reduced one-layer problem for the depleted electrolyte layer $0<x<1$, which reads as follows:

$$j^+ = c_x^+ + c^+\varphi_x = \text{const}, \quad 0 < x < 1, \tag{A10}$$

$$\varepsilon^2\varphi_{xx} = e^{\varphi} - c^+, \quad 0 < x < 1, \tag{A11}$$

$$\varphi(0) = \ln\left(\frac{2j^+}{e^V - 1}\right), \quad c^+(0) = \frac{\left(1 + \frac{j^+}{2}\right)}{j^+}(1 - e^{-V}), \tag{A12}$$

$$c^+(1) = 1, \quad \varphi(1) = 0. \tag{A13}$$

The rest of the analysis is similar to that of the problem [Eqs. (1)–(6)]. We reduce the formulation [Eqs. (A10)–(A13)] to a suitable boundary-value problem for inhomogeneous Painleve equation of second kind, whose solution yields the EDL dynamics under current. Let us note that for the quasiequilibrium regime, $V=O(1)$, ionic concentration profiles in both layers $-1<x<0$ and $0<x<1$, are antisymmetric, with the interface counterion concentration $c^+(0)$ equal unity. This symmetry breaks down with the appearance of the ESC zone. In Fig. 16(a) we present the current or voltage dependence together with the total electrolyte layer charge/versus voltage plot. Let us note the perfect coincidence of both plots, which means that in our toy model, with membrane's fixed charge absent, the charge of the electrolyte layer is proportional to the electric current. In Fig. 16(b) we plot the depleted electrolyte layer's charge versus voltage along with the QE-EDL charge versus voltage. We note a sharp decrease in the second plot with the appearance of the ESC zone.

APPENDIX B: REVIEW OF SOLUTIONS TO THE BASIC PROBLEM [Eqs. (14)–(18)] FOR VARIOUS RANGES OF VOLTAGE V

Scenario 1. Thin QE-EDL, $z_0=-O(\varepsilon^{-2/3})$, $x_0=-O(1)$, and $V=O(1)$.

We begin with the regime of a thin QE-EDL near the membrane surface $z=0$. In this case the integration of the basic problem [Eqs. (14)–(18)] yields (see Ref. [19])

$$F(z) = -\frac{1}{z - z_0} - \frac{4\sqrt{|z_0|}\left(2\frac{p_1}{|z_0|\varepsilon^{2/3}}(j^+)^{-2/3} - 1\right)e^{-z\sqrt{|z_0|}}}{\left(\sqrt{2\frac{p_1}{|z_0|\varepsilon^{2/3}}(j^+)^{-2/3}} + 1\right)^2 - \left(\sqrt{2\frac{p_1}{|z_0|\varepsilon^{2/3}}(j^+)^{-2/3}} - 1\right)^2 e^{-2z\sqrt{|z_0|}}}. \tag{B1}$$

Then, rewriting Eq. (B1) in outer variables we find

$$\varphi_x = \frac{1}{x - x_0} - \frac{1}{\varepsilon}\frac{4\sqrt{j^+x_0}\left(2\frac{p_1}{j^+x_0} - 1\right)e^{-x\sqrt{j^+x_0}/\varepsilon}}{\left(\sqrt{\frac{2p_1}{j^+x_0}} + 1\right)^2 - \left(\sqrt{2\frac{p_1}{j^+x_0}} - 1\right)^2 e^{-2x\sqrt{j^+x_0}/\varepsilon}} \tag{B2}$$

and

$$x_0 = -\frac{2\sqrt{p_1}}{j^+}e^{-V/2}. \tag{B3}$$

Finally, from the solution of the leading-order problem for Eqs. (1)–(6) valid for $x \gg \varepsilon$ we obtain

$$j^+ = 2(1 - \sqrt{p_1}e^{-V/2}). \tag{B4}$$

Scenario 2. Thick QE-EDL, $-\varepsilon^{-2/3} < O(z_0) < 1$, $-1 < O(x_0) \le -O(\varepsilon^{-2/3})$, and $O(V) < -\frac{4}{3}\ln\varepsilon$.

In this case in addition to the thin QE-EDL intrinsic scale $x=O(\varepsilon)$ there appears a new scale $x=O(\frac{\varepsilon}{\sqrt{|x_0|}})$, which for higher voltages $O(V)=\frac{4}{3}\ln\varepsilon$ transforms into the extended space charge scale $x=O(\varepsilon^{2/3})$. The following asymptotic expansion of Eq. (B1) implies the appearance of the thick component to the QE-EDL:

$$\varphi_x = 4\frac{\sqrt{-j^+x_0}}{\varepsilon}\cdot\frac{\exp\left(\frac{-x\sqrt{-j^+x_0}}{\varepsilon}\right)}{1 - \exp\left(\frac{-2x\sqrt{-j^+x_0}}{\varepsilon}\right)} - \frac{2}{x} + \frac{2}{x + \sqrt{2p_1}\varepsilon} - \frac{1}{x - x_0}. \tag{B5}$$

The solution of the problem [Eqs. (1)–(6)] in the EN bulk yields up to the leading order

$$x_0 = -2\sqrt{p_1}e^{-V/2}, \quad j^+ = 2. \tag{B6}$$

Scenario 3. Transition to nonequilibrium EDL. $z_0=O(1)$, $x_0=O(\varepsilon^{-2/3})$, and $V=-O(\frac{4}{3}\ln\varepsilon)$.

In this case the electric current density j^+ is up to the leading order given by Eq. (B4) and electric field is given by (see Ref. [19]):

$$\varphi_x = \frac{2}{x+\sqrt{2p_1\varepsilon}} - 2^{1/3}\varepsilon^{-2/3}F\left(\frac{2^{1/3}x}{\varepsilon^{2/3}}\right). \tag{B7}$$

First term in the composite solution [Eq. (B7)] represents the contribution of the thin EDL and the second of the extended space charge, where $F(z)$ is the basic singular Painleve solution to the following problem:

$$\frac{d^2F}{dz^2} = \frac{1}{2}F^3 + (z-z_0)F + 1, \tag{B8}$$

$$\left(F + \frac{2}{z}\right)\Big|_{z=0} = 0, \quad F(\infty) = 0. \tag{B9}$$

In order to simplify Eqs. (B8) and (B9), we define the regular part $G(z)$ of the singular Painleve solution as

$$G(z) = F(z) + \frac{2}{z}. \tag{B10}$$

Substitution of Eq. (B10) into problem [Eqs. (B8) and (B9)] yields the following boundary-value problem for $G(z)$:

$$\frac{d^2G}{dz^2} = \frac{1}{2}G^3 + \frac{6}{z^2}G - \frac{3}{z}G^2 + zG - 1 + z_0\left(\frac{2}{z} - G\right), \tag{B11}$$

$$G(0) = 0, \quad G(z) = \frac{2}{z} - \frac{1}{z-z_0} \quad \text{for} \quad z - z_0 \gg 1. \tag{B12}$$

The control parameter z_0 is determined via the solution of the following equation:

$$P(z_0) = -\frac{4}{3}\ln\varepsilon - V - \ln p_1 - \frac{4}{3}\ln j^+, \tag{B13}$$

where

$$P(z_0) \overset{\text{def}}{=} \int_0^\infty \left(G(z) - \frac{1}{z+1}\right)dz. \tag{B14}$$

Scenario 4. Developed microscopic nonequilibrium (extended) space charge zone $O(1) < z_0 < O(\varepsilon^{-2/3})$, $O(\varepsilon^{-2/3}) < x_0 < O(1)$, and $-O(\frac{4}{3}\ln\varepsilon) < V < O(1/\varepsilon)$.

In this case the electric current density j^+ is up to the leading order given by Eq. (B6) and electric field is given by (see Ref. [19]):

$$\varphi_x = \frac{2}{x+\sqrt{2p_1\varepsilon}} - \frac{2}{x} + \frac{2\sqrt{x_0}}{\varepsilon}\frac{2}{e^{2\sqrt{x_0}x/\varepsilon} - 1} - \varepsilon^{-2/3}2^{1/3}F_1[2^{1/3}\varepsilon^{-2/3}(x-x_0)], \tag{B15}$$

where F_1 is the following unique Painleve transcendent:

$$\frac{d^2F_1}{dz^2} = \frac{1}{2}F_1^3 + (z-z_0)F_1 + 1, \tag{B16}$$

$$(F_1 + \sqrt{-2z})|_{z=-\infty} = 0, \quad F_1(\infty) = 0. \tag{B17}$$

Substituting asymptotic expansion [Eqs. (B15)–(B17)] into Eq. (B13) and keeping leading-order terms yield

$$z_0 = \frac{3^{2/3}\left(V + \frac{4}{3}\ln\varepsilon\right)^{2/3}}{2}, \quad x_0 = \left(\frac{3\left(V + \frac{4}{3}\ln\varepsilon\right)\varepsilon}{4}\right)^{2/3}. \tag{B18}$$

Scenario 5. Macroscopic extended space charge zone $z_0 = O(\varepsilon^{-2/3})$, $x_0 = O(1)$, and $V = O(1/\varepsilon)$.

Keeping leading-order terms in Eq. (B15) we find

$$\varphi_x = \frac{2\sqrt{2x_0j^+}}{\varepsilon} \cdot \frac{1 - \sqrt{\frac{p_1}{x_0(j^+)^{1/3}} + 1}}{\left[1 + \sqrt{\frac{p_1}{x_0(j^+)^{1/3}} + 1}\right]e^{\sqrt{2x_0j^+}/\varepsilon} + 1 - \sqrt{\frac{p_1}{x_0(j^+)^{1/3}} + 1}} - \varepsilon^{-2/3}(j^+)^{1/3}F_1[(j^+)^{1/3}\varepsilon^{-2/3}(x-x_0)]. \tag{B19}$$

Integrating the outer EN bulk problem we find

$$j^+ = \frac{2}{1-x_0}, \tag{B20}$$

and substituting Eq. (B19) into Eq. (B18), keeping leading-order terms, we obtain the following algebraic equation for the edge of macroscopic extended space charge

$$\frac{x_0^3}{1-x_0} = \left(\frac{3V\varepsilon}{4}\right)^2. \tag{B21}$$

[1] I. Rubinstein, B. Zaltzman, A. Futerman, V. Gitis, and V. Nikonenko, Phys. Rev. E **79**, 021506 (2009).

[2] I. Rubinstein and B. Zaltzman, Phys. Rev. E **80**, 021505 (2009).

[3] B. M. Grafov and A. A. Chernenko, Dokl. Akad. Nauk SSSR **146**, 135 (1962).

[4] W. H. Smyrl and J. Newman, Trans. Faraday Soc. **63**, 207 (1967).

[5] R. P. Buck, J. Electroanal. Chem. **46**, 1 (1973).

[6] I. Rubinstein and L. Shtilman, J. Chem. Soc., Faraday Trans. 2 **75**, 231 (1979).

[7] A. V. Listovnichy, Elektrokhimiya **25**, 1651 (1989).

[8] V. V. Nikonenko, V. I. Zabolotsky, and N. P. Gnusin, Sov. Electrochem. **25**, 262 (1989).

[9] J. A. Manzanares, W. D. Murphy, S. Mafe, and H. Reiss, J. Phys. Chem. **97**, 8524 (1993).

[10] K. T. Chu and M. Z. Bazant, SIAM J. Appl. Math. **65**, 1485 (2005).

[11] I. Rubinstein and B. Zaltzman, Phys. Rev. E **62**, 2238 (2000).
[12] S. M. Rubinstein, G. Manukyan, A. Staicu, I. Rubinstein, B. Zaltzman, R. G. H. Lammertink, F. Mugele, and M. Wessling, Phys. Rev. Lett. **101**, 236101 (2008).
[13] H.-C. Chang and G. Yossifon, Biomicrofluidics **3**, 012001 (2009).
[14] S. S. Dukhin, Adv. Colloid Interface Sci. **35**, 173 (1991).
[15] S. S. Dukhin, N. A. Mishchuk, and P. B. Takhistov, Colloid J. USSR **51**, 616 (1989).
[16] S. J. Kim, Y. C. Wang, J. H. Lee, H. Jang, and J. Han, Phys. Rev. Lett. **99**, 044501 (2007).
[17] Y. Ben and H.-C. Chang, J. Fluid Mech. **461**, 229 (2002).
[18] G. Yossifon and H.-C. Chang, Phys. Rev. Lett. **101**, 254501 (2008).
[19] B. Zaltzman and I. Rubinstein, J. Fluid Mech. **579**, 173 (2007).
[20] S. Barany, N. A. Mishchuk, and D. C. Prieve, J. Colloid Interface Sci. **207**, 240 (1998).
[21] J. Balster, M. H. Yildirim, D. F. Stamatialis, R. Ibanez, R. G. H. Lammertink, V. Jordan, and M. Wessling, J. Phys. Chem. B **111**, 2152 (2007).
[22] R. B. Schoch, J. Y. Han, and P. Renaud, Rev. Mod. Phys. **80**, 839 (2008).
[23] A. Mani, T. A. Zangle, and J. G. Santiago, Langmuir **25**, 3898 (2009).
[24] J. R. Macdonald and S. W. Kenkel, J. Chem. Phys. **81**, 3215 (1984).
[25] M. S. Kilic, M. Z. Bazant, and A. Ajdari, Phys. Rev. E **75**, 021502 (2007); **75**, 021503 (2007).
[26] I. Rubinstein, I. Rubinstein, and E. Staude, PCH, Physico-Chem. Hydrodyn. **6**, 789 (1985).
[27] I. Rubinstein, *Electrodiffusion of Ions*, 1st ed. (SIAM, Philadelphia, 1990).
[28] J. R. Macdonald and C. A. Barlow, Jr., J. Chem. Phys. **36**, 3062 (1962).